Diode-pumped passively Q-switched self-frequency-doubled Nd:CNGS laser

XUZHAO ZHANG,[1] YING ZHOU,[1] ANATOL YASUKEVICH,[2] PAVEL LOIKO,[3] XAVIER MATEOS,[4] XINGUANG XU,[1] SHIYI GUO,[1,5] AND ZHENGPING WANG[1,*]

[1]State Key Laboratory of Crystal Materials, Shandong University, Jinan 250100, China
[2]Center for Optical Materials and Technologies (COMT), Belarusian National Technical University, 65/17 Nezavisimosti Ave., 220013 Minsk, Belarus
[3]ITMO University, Kronverkskiy pr., 49, 197101 Saint-Petersburg, Russia
[4]Física i Cristal·lografia de Materials i Nanomaterials (FiCMA-FiCNA)-EMaS, Dept. Química Física i Inòrganica, Universitat Rovira i Virgili (URV), Campus Sescelades, E-43007 Tarragona, Spain
[5]syguo@sdu.edu.cn
*zpwang@sdu.edu.cn

Abstract: With Cr^{4+}:YAG as a saturable absorber, a passively Q-switched self-frequency-doubled (SFD) laser based on a trigonal $Nd:Ca_3NbGa_3Si_2O_{14}$ (Nd:CNGS) silicate crystal was demonstrated for the first time. The maximum average output power at 532 nm was 16.2 mW, and the corresponding pulse repetition frequency, single pulse energy, pulse duration and peak power were 2.25 kHz, 7.2 µJ, 13.7 ns, 0.53 kW, respectively. We also present a rate-equation model of such a passively Q-switched SFD laser showing a good agreement with the experiment. Nd:CNGS is a promising pulse SFD material for miniature all-solid-state visible light sources.

References and links

1. C. Kränkel, D.-T. Marzahl, F. Moglia, G. Huber, and P. W. Metz, "Out of the blue: Semiconductor laser pumped visible rare-earth doped lasers," Laser Photonics Rev. **10**(4), 548–568 (2016).
2. H. Yu, N. Zong, Z. Pan, H. Zhang, J. Wang, Z. Wang, and Z. Xu, "Efficient high-power self-frequency-doubling Nd:GdCOB laser at 545 and 530 nm," Opt. Lett. **36**(19), 3852–3854 (2011).
3. P. Dekker, J. M. Dawes, J. A. Piper, Y. Liu, and J. Wang, "1.1 W CW self-frequency-doubled diode-pumped Yb:YAl$_3$(BO$_3$)$_4$ laser," Opt. Commun. **195**(5-6), 431–436 (2001).
4. X. Z. Zhang, Y. Zhou, J. Y. Ren, D. Z. Lu, H. H. Yu, Z. P. Wang, S. Y. Guo, and X. G. Xu, "Growth, thermal and laser properties of a new self-frequency-doubling Yb:CNGS crystal," CrystEngComm **18**(28), 5338–5343 (2016).
5. P. Loiko, J. M. Serres, X. Mateos, K. Yumashev, A. Yasukevich, V. Petrov, U. Griebner, M. Aguiló, and F. Díaz, "Sub-nanosecond Yb:KLu(WO$_4$)$_2$ microchip laser," Opt. Lett. **41**(11), 2620–2623 (2016).
6. C. Luan, X. Y. Zhang, K. J. Yang, J. Zhao, S. Z. Zhao, T. Li, W. C. Qiao, H. W. Chu, J. P. Qiao, J. Wang, L. H. Zheng, X. D. Xu, and J. Xu, "High-peak power passively Q-switched 2-µm laser with MoS$_2$ saturable absorber," IEEE J. Sel. Top. Quantum Electron. **23**(1), 1600105 (2017).
7. R. Abe, J. Kojou, K. Masuda, and F. Kannari, "Cr^{4+}-doped Y$_3$Al$_5$O$_{12}$ as a saturable absorber for a Q-switched and mode-locked 639-nm Pr^{3+}-doped LiYF$_4$ laser," Appl. Phys. Express **6**(3), 032703 (2013).
8. H. Tanaka, R. Kariyama, K. Iijima, K. Hirosawa, and F. Kannari, "Saturation of 640-nm absorption in Cr^{4+}:YAG for an InGaN laser diode pumped passively Q-switched Pr^{3+}:YLF laser," Opt. Express **23**(15), 19382–19395 (2015).
9. J. Bartschke, K. J. Boller, R. Wallenstein, I. V. Klimov, V. B. Tsvetkov, and I. A. Shcherbakov, "Diode-pumped passively Q-switched self-frequency-doubling Nd:YAB laser," J. Opt. Soc. Am. B **14**(12), 3452–3456 (1997).
10. F. Mougel, G. Aka, A. Kahn-Harari, H. Hubert, J. M. Benitez, and D. Vivien, "Infrared laser performance and self-frequency doubling of Nd:Ca$_4$GdO(BO$_3$)$_3$ (Nd:GdCOB)," Opt. Mater. **8**(3), 161–173 (1997).
11. D. A. Hammons, M. Richardson, B. H. T. Chai, A. K. Chin, and R. Jollay, "Scaling of longitudinally diode-pumped self-frequency-doubling Nd:YCOB lasers," IEEE J. Quantum Electron. **36**(8), 991–999 (2000).
12. X. Y. Zhang, S. Z. Zhao, Q. P. Wang, S. J. Zhang, L. K. Sun, X. M. Liu, S. J. Zhang, and H. C. Chen, "Passively Q-switched self-frequency-doubled Nd^{3+}:GdCa$_4$O(BO$_3$)$_3$ laser," J. Opt. Soc. Am. B **18**(6), 770–779 (2001).

13. X. T. Zhang, X. Z. Zhang, S. Y. Guo, J. L. He, K. Z. Han, F. Lou, B. T. Zhang, R. H. Wang, and X. M. Liu, "Growth and optical properties of a new CGG-type laser crystal Nd^{3+}:CNGS," Opt. Mater. Express **5**(5), 977–985 (2015).

14. F. F. Chen, F. P. Yu, S. Hou, Y. Q. Liu, Y. Zhou, X. Z. Shi, H. W. Wang, Z. P. Wang, and X. Zhao, "Crystal growth and characterization of CTGS and Nd:CTGS for self-frequency-doubling applications," CrystEngComm **16**(44), 10286–10291 (2014).

15. N. Pavel, J. Saikawa, and T. Taira, "Diode end-pumped passively Q-switched Nd:YAG laser intra-cavity frequency doubled by LBOcrystal," Opt. Commun. **195**(1-4), 233–240 (2001).

16. Y. Yu, J. Wang, H. Zhang, Z. Wang, H. Yu, and M. Jiang, "Continuous wave and Q-switched laser output of laser-diode-end-pumped disordered Nd:LGS laser," Opt. Lett. **34**, 467–469 (2009).

17. G. J. Spühler, R. Paschotta, R. Fluck, B. Braun, M. Moser, G. Zhang, E. Gini, and U. Keller, "Experimentally confirmed design guidelines for passively Q-switched microchip lasers using semiconductor saturable absorbers," J. Opt. Soc. Am. B **16**(3), 376–388 (1999).

18. A. S. Yasukevich, P. Loiko, N. V. Gusakova, J. M. Serres, X. Mateos, K. V. Yumashev, N. V. Kuleshov, V. Petrov, U. Griebner, M. Aguiló, and F. Díaz, "Modelling of graphene Q-switched Tm lasers," Opt. Commun. **389**, 15–22 (2017).

19. R. Lan, P. Loiko, X. Mateos, Y. Wang, J. Li, Y. Pan, S. Y. Choi, M. H. Kim, F. Rotermund, A. Yasukevich, K. Yumashev, U. Griebner, and V. Petrov, "Passive Q-switching of microchip lasers based on Ho:YAG ceramics," Appl. Opt. **55**(18), 4877–4887 (2016).

20. L. Chen, S. Han, Z. Wang, J. Wang, H. Zhang, H. Yu, S. Han, and X. Xu, "Controlling laser emission by selecting crystal orientation," Appl. Phys. Lett. **102**(1), 011137 (2013).

21. N. I. Leonyuk and L. I. Leonyuk, "Growth and characterization of $RM_3(BO_3)_4$ crystals," Prog. Cryst. Growth Charact. Mater. **31**(3–4), 179–278 (1995).

1. Introduction

To date, there are two most convenient ways to obtain compact all-solid-state laser sources emitting in the visible: one is blue laser pumped Pr^{3+}, Sm^{3+}, Tb^{3+}, Dy^{3+}, Ho^{3+} and Er^{3+} lasers [1], and the other is self-frequency-doubling of near-IR Nd^{3+} or Yb^{3+} lasers [2–4]. For the continuous-wave (CW) operation, both methods require only the laser medium in the resonator, which means that one can design compact, portable and cheap oscillators, incl. the ones based on microchip concept. As for the Q-switched operation, the most convenient approach is to insert into the laser resonator a proper saturable absorber (SA) to realize high peak power pulsed output [5, 6]. Recently, a commercial SA, the Cr^{4+}:YAG crystal, has been applied to the blue laser pumped Pr^{3+}:YLF lasers [7, 8]. With a three-mirror V-shaped cavity, the largest pulse energy of 6.2 µJ and the highest peak power of 64 W were obtained at 640 nm [8]. For Cr^{4+}:YAG, although the saturable absorption at 522 nm was also observed in a Z-scan measurement [7], the direct Q-switching application to the green transition of solid-state lasers has not been realized so far.

The state-of-the-art SA for ~1 µm lasers, Cr^{4+}:YAG once was used in diode-pumped self-frequency-doubled (SFD) Nd:YAB laser to generate green Q-switched pulses. An energy of 1 µJ at a repetition rate of 45 kHz was obtained at 531 nm, corresponding to a peak power of 148 W [9]. The large stimulated-emission cross-section (2.0×10^{-19} cm^2) and short upper-laser-level lifetime (60 µs) of Nd:YAB led to a small energy storage capability, which elevated the repetition rate and limited the pulse energy and the peak power. Nd:GdCOB and Nd:YCOB are the two SFD crystals which obtained rapid development in the recent years. They exhibited excellent CW SFD characteristics, while for passively Q-switched (PQS) operation their short upper-level lifetime of ~100 µs [10, 11] is unfavorable. By time now, only flash lamp pumped PQS laser has been realized [12]. To improve the performance of PQS SFD laser, it is necessary to find suitable materials which can cooperate with Cr^{4+}:YAG, i.e. have long upper-level lifetime.

In this paper, we report a diode-pumped $Nd:Ca_3NbGa_3Si_2O_{14}$ (Nd:CNGS) SFD laser PQS by a Cr^{4+}:YAG SA. For Nd:CNGS, the stimulated-emission cross-section at 1064 nm is 3.0 ~6.8×10^{-20} cm^2 depending on the polarization and the upper-laser-level lifetime is 256 µs [13]. This indicates that Nd:CNGS possesses excellent energy storage capability, which is proved by the PQS laser experiments. The maximum SFD pulse energy is 7.2 µJ, and the highest peak power is 0.53 kW. These are the record characteristics for a diode-pumped PQS

SFD laser up to now. The performance of the developed laser was theoretically analyzed within a model of a four-level laser PQS by a "slow" SA exhibiting the excited-state absorption (ESA).

2. Laser set-up

The scheme of the laser set-up is shown in Fig. 1(a). The laser crystal was a 13 mm-thick 0.5 at.% Nd:CNGS crystal cut along the type-I phase-matching direction ($\theta = 35.8°$, $\varphi = 30.0°$) for the ~1064 nm fundamental laser emission, as calculated from the Sellmeier equations for the principal refractive indices [13]. Nd:CNGS is a trigonal crystal (sp. gr. $P321$, point group 32) and, thus, it is optical uniaxial. Considering the previously reported nonlinear optical coefficient d_{11} of 0.72 ± 0.01 pm/V for an isostructural Nd:CTGS crystal [14], the effective nonlinear optical coefficient for type-I phase-matching direction is $d_{eff} = d_{11}cos^2\theta sin3\varphi = 0.47$ pm/V. The Nd:CNGS crystal was wrapped with indium foil and mounted in a Cu holder which was water-cooled to 15 °C. Both input and output faces of the Nd:CNGS crystal were antireflection (AR) coated at 808, 1064 and 532 nm. The SA was a 0.7 mm-thick Cr^{4+}:YAG crystal with both surfaces AR-coated for 1064 nm. The initial (small-signal) transmission of the SA T_{SA} was 93.7% at 1064 nm.

A flat-flat laser resonator was used with a geometrical length of 20 mm. The flat pump mirror (PM) was coated for high transmission (HT) at 808 nm and high reflectance (HR) at 1064 and 532 nm. The flat output coupler (OC) was coated for HT at 532 nm and HR at 1064 nm. The laser crystal was placed closer to the PM. The Cr^{4+}:YAG SA was inserted between the laser crystal and the OC. We used a fiber-coupled AlGaAs laser diode (LD, Limo 70-F200-DL808-T2M3P0, fiber core diameter: 200 μm, numerical aperture, N.A.: 0.22) as a pump source. It emitted unpolarized output at ~808 nm. An optical coupling system (OCS) was used to collimate and focus the pump beam into the laser crystal with a magnification of 1:1 so that the pump spot radius w_p was 100 μm (the confocal parameter, $2z_R = 1.67$ mm, M^2 parameter for the pump beam: 85).
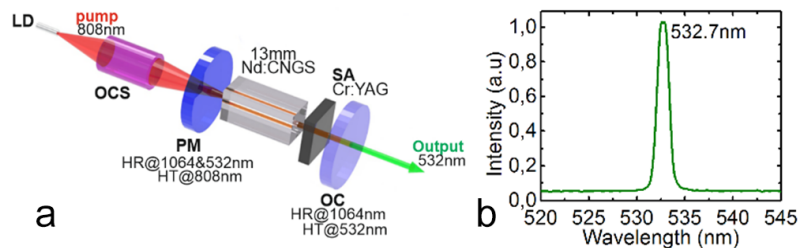

Fig. 1. (a) Experimental setup of the PQS SFD Nd:CNGS laser: LD – laser diode, OCS – optical coupling system, PM – pump mirror, SA – saturable absorber, OC – output coupler; (b) typical emission spectrum of this laser.

The output power was measured by a powermeter (Powermax 500D, Molectron) using a cut-off filter for the green output, and the temporal behavior of the Q-switched laser output were recorded by a 1 GHz digital oscilloscope (DPO 7104, Tektronix). The spectrum of green laser emission was measured with an optical spectrum analyzer (HR 4000, Ocean Optics), see Fig. 1(b).

3. Experimental result and discussion

3.1 Laser performance

At first, we studied the performance of the laser in the CW mode (when the Cr^{4+}:YAG SA was removed from the resonator), see Fig. 2(a). At an absorbed pump power P_{abs} of 3.95 W, the maximum CW green power of 72.8 mW was achieved. The pump absorption of the laser crystal measured under non-lasing conditions varied in the range 72%...69% depending on the

pump level due to a slight temperature drift of the emission wavelength of the AlGaAs laser diode. For the PQS laser, the average output power P_{out}, the pulse repetition frequency (PRF), and the pulse duration $\Delta\tau$ (determined as the full width at half maximum, FWHM) were measured directly, while the single pulse energy E_{out} was determined as P_{out}/PRF, and the peak power P_{peak} - as $E_{out}/\Delta\tau$. The results are shown in Fig. 2(a)-2(c). It could be seen that the threshold pump power increased greatly compared to the CW operation situation. For intracavity passively Q-switched lasers it is a common experimental phenomenon, which appears in frequency doubling or fundamental laser operations [15, 16]. With the increase of P_{abs}, the pulse energy increased from 3.1 to 7.2 µJ and the PRF – from 1.3 to 2.25 kHz while the pulse duration only slightly shortened from 15.8 to 13.7 ns. At the maximum P_{abs} = 2.95 W, the maximum average green output power amounted to 16.2 mW, and the corresponding peak power was 0.53 kW. Further increasing the pump power, the SFD output saturated, which is attributed to the thermal effects in the laser medium and in the SA. The typical oscilloscope trace of the single Q-switched pulse corresponding to the maximum SFD green output is shown in Fig. 2(d). No multi-pulse behavior has been observed. The inset of Fig. 2(d) is the corresponding pulse train with a repetition rate of 2.25 kHz. It should to be noted that the present crystal length of Nd:CNGS (13 mm) and initial transmittance of Cr:YAG (93.7%) were optimized experimental parameters. When 6 mm, 9 mm long Nd:CNGS crystals or T_0 = 97%, 85% Cr:YAG SAs were used in this experiment, their passively Q-switched SFD results were entirely inferior to the data of Fig. 2. The polarization of the SFD output was ordinary (o), as determined by a Gran-Taylor prism. It was orthogonal to the polarization of fundamental emission (extraordinary (e)), measured in a separate laser experiment without SFD. In this way, the type-I phase-matching process (ee-o) was observed.
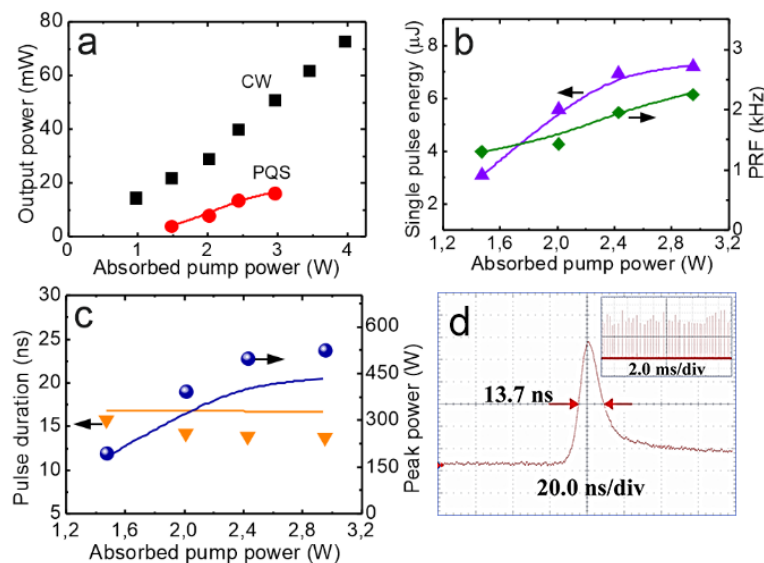

Fig. 2. SFD Nd:CNGS laser: (a) output power for CW and PQS operation modes; (b) single pulse energy and pulse repetition frequency (PRF), (c) pulse duration and peak power, (d) oscilloscope trace of the single Q-switched pulse at P_{abs} = 2.95 W (for PQS operation mode). *Inset*: the corresponding pulse train with a repetition rate of 2.25 kHz. *Symbols* in (a)-(c) – experimental data, *curves* – numerical modelling.

In addition to the experimental set-up depicted in Fig. 1(a), we tried other configurations, including other pump source and position of the SA. Using a fiber-coupled LD with a 100 µm fiber core (Limo35-F100-DL808-LM) as the pump source, at a similar pump level of P_{abs} = 3 W, the average output power, PRF, pulse energy and pulse duration of the PQS SFD laser were 37.5 mW, 9.60 kHz, 3.91 µJ and 22.2 ns, respectively. Besides the higher P_{out} than that

from Fig. 2, the peak power in this case was lower, 0.18 kW. From the theory of the PQS laser, it is known that the pulse energy and peak power are proportional to the laser mode area [12, 17]. For the flat-flat cavity used in this work, smaller pump spot size will lead to a smaller laser mode area and decreased the energy storage capability.

Next, using the same LD with a 100 μm fiber core, we varied the SA position, i.e. placed the Cr^{4+}:YAG crystal between the Nd:CNGS crystal and the PM and recorded the PQS SFD laser performance. At P_{abs} = 3 W, the maximum average output power reached 64.6 mW, corresponding to a PRF of 23.34 kHz, and a pulse energy of 2.77 μJ. Considering the pulse duration of 27.9 ns, the peak power was only 0.10 kW. Consequently, under the same pump conditions, the scheme where the Cr^{4+}:YAG SA is inserted between the laser crystals and the OC, Fig. 1(a), provides large pulse energy, shorter pulse duration, and higher peak power, while the scheme with the SA positioned between the laser crystal and the PM allows one to achieve higher average output power and PRF.

This can be explained as following. For the latter scheme, although it introduced some absorption loss for the pump light (~5%), it effectively avoided the absorption of the green SFD emission in the Cr^{4+}:YAG SA, which is a limitation of the former set-up. So, higher average output power was obtained. The difference in $\Delta\tau$ and E_{out} for the two set-ups is most probably due to the asymmetry of the laser mode in the resonator due to the thermal lens leading to different bleaching conditions for the SA.

As a further improvement of the laser set-up depicted in Fig. 1(a), a dichroic mirror coated for HT at the fundamental wavelength and HR for the SFD emission can be inserted between the laser crystal and the Cr:YAG SA at an angle of 45°, which will allow one to avoid the absorption of green emission in the SA.

3.2 Numerical modelling

The output characteristics of the passively Q-switched SFD Nd:CNGS/Cr^{4+}:YAG laser were theoretically investigated with a four-level laser model which was Q-switched by a "slow" SA. For this purpose, the model from [18, 19] has been modified. The rate equations were written for three variables: (i) I_L – radiation intensity in the laser crystal at the fundamental laser frequency v_L, (ii) N_3 - population of the upper laser level (for the four-level laser system, we assume $N_2 = N_4 = 0$, so $N_1 + N_3 = N_{Nd}$), and (iii) N_{GS} - population of the ground-state (GS) of the SA ($N_{GS} + N_{ES} = N_{SA}$):

$$\frac{dI_L}{dt} = \frac{c\mu}{n_1}[k_L - k_{loss} - k_{loss}^{SH} - \frac{l_{SA}}{l_{AM}}k_{SA}]I_L + I'_{noise},\tag{1a}$$

$$\frac{dN_3}{dt} = \frac{I_p}{hv_p}k_p - \frac{I_L}{hv_L}k_L - \frac{N_3}{\tau},\tag{1b}$$

$$\frac{dN_{GS}}{dt} = -\frac{I_L}{hv_L}\sigma_{GSA}N_{GS} + \frac{N_{SA} - N_{GS}}{\tau_{rec}}.\tag{1c}$$

Here, k_L is the gain coefficient, k_{loss} is the resonator loss coefficient at the laser frequency v_L, k^{SH}_{loss} is the effective loss coefficient related to the SFD, and k_{SA} is the loss coefficient in the SA:

$$k_L = N_3\sigma_{SE}^L,\tag{2}$$

$$k_{loss} = -\frac{1}{2l_{AM}}[\ln(1-T_{OC}) + \ln(1-L)],\tag{3}$$

$$k_{\text{loss}}^{\text{SH}} = \frac{\xi}{2l_{\text{AM}}} I_L, \text{ where } \xi = \frac{2\pi^2 d_{\text{eff}}^2 l_{\text{AM}}^2}{\varepsilon_0 n_1^2 n_2 \lambda_2^2}, \tag{4}$$

$$k_{\text{SA}} = \sigma_{\text{GSA}} N_{\text{GS}} + \sigma_{\text{ESA}} (N_{\text{SA}} - N_{\text{GS}}). \tag{5}$$

The resonator and material parameters used in the formulas are as follows: $\mu = l_{\text{AM}} n_1 / l_c$ is the resonator filling factor; l_{AM} and l_{SA} are the lengths of the active material (AM) and SA, respectively; n_1 and n_2 are the refractive indices of the AM at the fundamental and second-harmonic (λ_2) wavelengths, respectively; l_c is the optical length of the resonator; v_p is the pump frequency; T_{OC} is the transmission of the output coupler and L is the round trip passive intracavity loss; I'_{noise} is the rate of noise intensity, see details in [18]; $\sigma_{\text{SE}}^{\text{L}}$ is the stimulated-emission (SE) cross-section of the AM at the laser frequency; σ_{GSA} and σ_{ESA} are the ground- and excited-state absorption cross-sections of the SA, τ is the lifetime of the upper laser level (Nd^{3+}), τ_{rec} is the recovery time of the initial absorption of the SA, d_{eff} is the effective nonlinear coefficient of the AM. The fundamental constants: c is the light velocity, ε_0 is the vacuum permittivity, and h is the Planck constant.

The average pump intensity in the AM, I_p, is expressed as:

$$I_p = \frac{P_{\text{inc}}}{\pi w_p^2} \frac{1 - \exp(-k_p l_{\text{AM}})}{k_p l_{\text{AM}}}, \text{ where} k_p = (N_{\text{Nd}} - N_3) \sigma_{\text{abs}}^p. \tag{6}$$

Here, P_{inc} is the incident pump power and w_p is the pump spot radius, k_p is the absorption coefficient for the pump radiation and σ_{abs}^p is the absorption cross-section of the AM at the pump frequency v_p. The pump and laser intensities, populations, loss and gain coefficients are considered as averaged over the crystal volume.

The solution of the system of rate equations yields a time-dependent intracavity laser intensity $I_L(t)$ which is used to calculate the output green laser power:

$$P_{\text{out}}^{\text{SH}}(t) = V_L k_{\text{loss}}^{SH} I_{\text{L}}(t) = \frac{\pi w_{\text{L}}^2}{4} \xi I_{\text{L}}(t)^2. \tag{7}$$

Here, V_L (w_L) is the volume (radius) of the laser mode in the AM. From the time-dependent $P_{\text{out}}^{\text{SH}}(t)$, we calculated the pulse duration (as full width at half maximum, i.e. FWHM), the pulse energy and the PRF for the Q-switched pulses.

The material parameters of the AM and SA used for the calculations are listed in Table 1. It should be noted that the $\sigma_{\text{SE}}^{\text{L}}$ is the SE cross-section at type-I SFD direction, (35.8°, 30.0°). It was calculated as $\sigma_{\text{SE}}^{\text{L}} = \sigma_\pi \cos^2(\theta) + \sigma_\sigma \sin^2(\theta)$ [20], where σ_π and σ_σ are the SE cross-sections for the π and σ polarizations, respectively, derived with the Füchtbauer–Ladenburg (F-L) equation [13].

Table 1. Material and Laser Cavity Parameters Used for the Calculations.

Parameter	Value	Parameter	Value	Parameter	Value
AM		SA		Cavity	
l_{AM}	13 mm	l_{SA}	0.7 mm	$\lambda_{\text{L}}(\lambda_2)$	1064 (532) nm
$n_1(n_2)$	1.80 (1.84)	n_{SA}	1.81	λ_p	808 nm
N_{Nd}	0.5×10^{20} cm^{-3}	σ_{GSA}	3.5×10^{-18} cm^2	w_{L}	50±5 μm
$\sigma_{\text{SE}}^{\text{L}}$	4.0×10^{-20} cm^2	σ_{ESA}	0.3×10^{-18} cm^2	w_p	160±40 μm
σ_{abs}^p	$\sim2\times10^{-20}$ cm^2	τ_{rec}	3.5 μs	L	$\sim2\%$
τ	256 μs			l_{geom}	20 mm
d_{eff}	0.3±0.1 pm/V				

The modelling results are shown in Figs. 2(a)-2(c) (as curves) in terms of pulse characteristics and in Fig. 3 in terms of the calculated pulse trains and single Q-switched pulses. The model correctly describes the increase of the pulse repetition frequency (PRF) and peak power and shortening of the pulse duration with the increase of the absorbed pump

power P_{abs}, as well as the temporal shape of the single Q-switched pulses. In particular, for P_{abs} = 2.95 W, it predicts generation of 7.2 μJ / 16.7 ns pulses (green emission) at a PRF = 2.28 kHz corresponding to an average output power of 16.5 mW. These results agree well with the experimental data of Figs. 2(a)-2(c). The best agreement between the experimental and calculated pulse characteristics have been observed for d_{eff} = 0.3 ± 0.1 pm/V that is in reasonable agreement with the value estimated above.
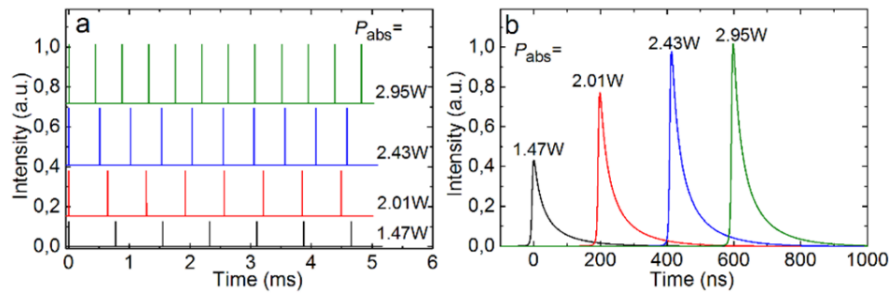

Fig. 3. Calculated (a) pulse trains and (b) single Q-switched pulses for the green output of the PQS SFD Nd:CNGS laser. In (a), the pulse trains are shifted for the sake of clarity, the time is counted from the moment of appearance of the first pulse. In (b), the time scale for the single pulses is shifted.

4. Conclusion

In this paper, we report on first PQS SFD Nd:CNGS green laser. It is using a laser crystal cut along the type I phase-matching direction and a Cr^{4+}:YAG crystal as a SA. The best pulse characteristics (energy/duration) are 7.2 μJ/13.7 ns at a repetition rate of 2.25 kHz resulting in > 0.5 kW peak power. The performance of this laser is modelled within a four-level laser model with a "slow" SA resulting in good agreement with the experiment.

The self-frequency doubling is a simple and efficient approach towards the development of visible lasers. Compared to the standard SHG-setups, SFD laser component is simpler, cheaper, and has fewer production procedures, because no individual NLO medium is needed. Combined with LD pumping and passive Q-switching, compact, all-solid-state low-cost pulsed SFD lasers can be produced. To date, among all the SFD crystals, only Nd:YAB was used in a LD-pumped PQS SFD green laser [9]. The relatively short lifetime of the upper laser level of Nd^{3+} in YAB limited its pulsed performance. Besides, the flux growth of Nd:YAB is complicated and it is difficult to obtain high quality crystals [21]. Comparing with Nd:YAB, Nd:CNGS possesses much longer upper laser level lifetime (~4 times), which means better energy storage capability, larger pulse energy, and higher peak power. These characteristics are verified by the results achieved in this paper. In addition, large-volume, high-quality Nd:CNGS crystals can be grown by the Czochralski (Cz) pulling method in a short time. All of these properties indicate that Nd:CNGS is a promising SFD laser material. We believe that it is suitable for making cheap, simple, miniature green pulsed lasers which can find applications in such areas as three-dimensional laser scanning, data storage, contamination detection, spectroscopy and microsurgery.